ACS Sustainable Chemistry & Engineering

Letter

pubs.acs.org/journal/ascecg

Ultrasmall Copper Nanoparticles Synthesized with a Plant Tea Reducing Agent

Aaron D. Brumbaugh, Katelyn A. Cohen, and Sarah K. St. Angelo*

Department of Chemistry, Dickinson College, P.O. Box 1773, Carlisle, Pennsylvania 17013, United States

Supporting Information

ABSTRACT: Ultrasmall copper nanoparticles were synthesized using lemongrass tea as a green reducing agent. The one-pot, aqueous, room-temperature reaction produces nanoparticles with diameters of 2.90 ± 0.64 nm. UV−vis spectroscopy shows the ultrasmall nanoparticles are nonplasmonic. FTIR spectroscopy indicates that oxygen-containing functional groups in the lemongrass tea are present in the nanoparticle reaction mixture. High-resolution transmission electron microscopy (HR-TEM) was used to confirm that the nanoparticles are Cu, as indicated by the lattice spacing measurements for the (111), (200), and (220) lattice planes of Cu. The nanoparticles are transferrable from water to hexane with octadecanethiol (ODT) as a phase transfer agent. X-ray energy dispersive spectroscopy (EDS) conducted during TEM analysis confirms the presence of copper in the nanoparticle samples and indicates that the phase-transferred nanoparticles have relatively less material associated with lemongrass tea than the as-synthesized sol.

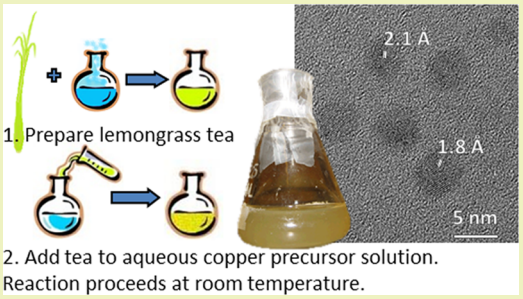

KEYWORDS: *Ultrasmall nanoparticles, Copper nanoparticles, Green nanoparticle synthesis, HR-TEM, EDS*

INTRODUCTION

Copper nanoparticles are of increasing interest particularly due to their potential use in catalysis, photovoltaics, energy applications, and metallic inks.[1−8] Copper has the advantages of lower cost and increased abundance relative to common catalytic materials, such as platinum or gold. The greater surface area afforded by nanoparticles when compared to bulk metal is further increased as nanoparticle diameter is decreased. Many properties of nanomaterials are size dependent; hence, new methods for producing ultrasmall nanoparticles are of interest so that properties relying on nanoparticle size may be investigated and exploited. Furthermore, ultrasmall nanoparticles and metal clusters bridge the size scales of molecular species and larger nanoparticles or microparticles. Ultrasmall nanoparticles may link molecular-scale materials with those of larger dimensions and include the physical and chemical properties defined by the size and composition of ultrasmall nanoparticles.

As a relatively new category within a still-growing field of nanochemistry, "ultrasmall" nanoparticles have been variously defined in the literature, and as has been noted recently, there is not yet an established definition.[9] At one extreme, isotropic nanoparticles with diameters of ∼10 nm have been categorized as ultrasmall and include gold,[10,11] tin,[12] tin oxide,[13] lanthanide-doped nanocrystals,[14] and silica nanoparticles.[15] A recent review of nanoparticles has used the 10 nm dimension as a primary criterion for a material being considered ultrasmall.[16] Another dimension used to define ultrasmall nanoparticles is ∼5−6 nm diameters, and nanoparticles having those diameters that have been categorized as ultrasmall include yttrium fluoride,[17] iron oxide,[18,19] and tin.[20] Ultrasmall nanoparticles with diameters of 2−4 nm include gold,[9,21,22] silver,[23] copper,[24] and iron−platinum.[25] Nanoparticles with diameters of less than 2 nm and atomically precise clusters have also been classified as being ultrasmall nanoparticles.[9,26−29] The synthesis of copper nanoparticles in the ultrasmall range, considered here to have diameters less than 5 nm, can be problematic due to the tendency of small nanoparticles to agglomerate or ripen to form larger particles and notably in the case of copper to form oxides. The variety of syntheses for ultrasmall copper nanoparticles includes use of surfactant templates and carbon nanotube scaffolding with citrate reduction,[30] EDTA-mediated reduction of $Cu(OH)_2$ in the presence of polyvinylpyrrolidone,[24] surfactant-mediated hydrazine-citrate reduction,[31] and the $NaBH_4$ reduction of copper (pH ∼13) in the presence of surfactant within a millifluidic reactor.[32] Recently, greener syntheses of metallic nanoparticles of various sizes and shapes have been burgeoning with gold and silver;[33−37] however, there are fewer examples of copper nanoparticle syntheses using greener methods.[38−40] Greener methods for producing ultrasmall copper nanoparticles are even more limited.[41,42]

Herein, the room-temperature synthesis of ultrasmall copper nanoparticles is demonstrated with an aqueous tea of lemongrass stalks. Lemongrass was considered for its ability to form copper nanoparticles because of previous work documenting its use in the formation of gold nanoplatelets,[43,44] the role of lemongrass in the formation of gold−silver core−shell nanoplatelets,[45] and the demonstrated lemongrass-based synthesis of silver nanoparticles.[46] As the coinage metals of

Received: March 11, 2014
Published: July 3, 2014

 © 2014 American Chemical Society

gold, silver, and copper are commonly considered as a group, this work aims to add copper nanoparticles to the repertoire of lemongrass-mediated nanoparticle synthesis. Specifically, this work presents the lemongrass-reduction of copper with a simple, low-cost, low-energy, and low-hazard aqueous synthetic method. The nanoparticles are characterized with spectroscopic techniques and transmission electron microscopy (TEM) methods, including in situ elemental analysis. The nanoparticles are transferable to hexane via derivatization with an alkanethiol and are fully reduced Cu (0) with no evidence of associated oxides.

EXPERIMENTAL SECTION

A tea of lemongrass (*Cymbopogon citratus*) was prepared in a similar manner to a procedure used elsewhere for the synthesis of gold nanoplatelets.[43] Lemongrass stalks were purchased at a local market, washed, and finely chopped. The lemongrass pieces were added to boiling deionized water in a mass to volume ratio of 1 g lemongrass pieces to 5 mL water. The mixture was allowed to boil for 10 min, removed from the heat, and allowed to cool to room temperature. The mixture was passed through fast filter paper to remove the lemongrass solids and then was filtered through a membrane filter having 0.2 μm pores. The filtrate was stored at 4 °C and was used within 2 weeks of preparation. The unadjusted pH of the lemongrass tea was 5.2 ± 0.1, as measured by a calibrated Accumet XL20 pH meter.

All chemicals were used as received. The ultrasmall copper nanoparticles were prepared by combining aqueous 1 mM $CuSO_4 \cdot 5H_2O$ (ACS grade, Mallinckrodt Chemicals) with aqueous lemongrass tea. A typical preparation was composed of 70% 1 mM $CuSO_4$, 29% lemongrass tea, and 1% added deionized water by volume. The solutions were combined, mixed well, and allowed to react on the lab bench with constant magnetic stirring. The solutions became yellow over the course of 3 days of reaction under ambient temperature and lighting conditions. Subsequent analyses, sample preparation, and aqueous−organic phase transfer were conducted at this time. For aqueous−organic phase transfer experiments, 1-octadecanethiol (ODT) was purchased from Sigma-Aldrich, and isopropanol and hexanes were purchased from BDH. ODT (1 mM, 0.2 mL) in isopropanol was added to 1 mL of the prepared nanoparticles. Hexane (0.2 mL) was added to the nanoparticle−ODT solution and mixed well. A small volume of water was added to reform separate aqueous and organic phases. A transmission electron microscopy (TEM) grid (carbon-coated Ni grid, Electron Microscopy Sciences) was dipped into the hexane layer and allowed to dry. TEM, high-angle annular dark field scanning TEM (HAADF STEM), high-resolution TEM images (HR-TEM), and in situ elemental analysis via X-ray energy dispersive spectroscopy (EDS) were performed with a JEOL 2010-F transmission electron microscope operated with an accelerating voltage of 200 kV. Samples of the as-synthesized sol were prepared for TEM imaging by drop-coating the aqueous nanoparticle solutions onto carbon-coated Ni TEM grids and allowing them to air dry.

Ultraviolet−visible (UV−vis) spectroscopy was performed with a Jasco V-670 spectrophotometer. Fourier transform infrared (FTIR) spectra were acquired with a Thermo-Nicolet Avatar 360 FTIR. Samples were prepared for FTIR analysis by freeze-drying the aqueous samples, grinding the dried samples with KBr, and forming KBr pellets.

The percent yield of nanoparticles was determined by centrifuging a sample of the as-synthesized sol at 13,700*g* for 10 min (10,000 rpm Beckman Centrifuge with a Beckman JA-17 rotor). The supernatant and pellet were separately digested with concentrated nitric acid and subsequently diluted with deionized water. The solutions were evaluated for copper content at 327.4 nm with a 0.2 nm slit width using a hollow cathode copper lamp in a Varian SpectrAA 55B atomic absorption spectrometer.

RESULTS AND DISCUSSION

A representative UV−vis spectrum of an aqueous nanoparticle mixture is shown in Figure 1a. Higher overall apparent

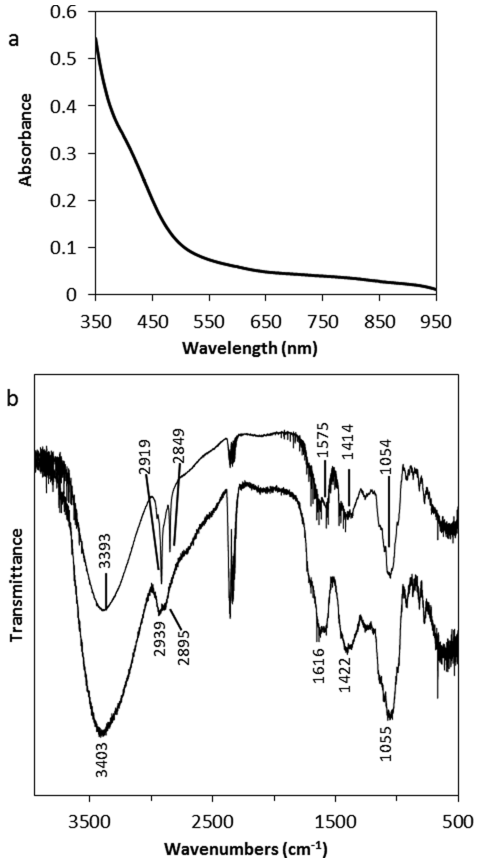

Figure 1. (a) UV−vis spectrum of the as-synthesized ultrasmall copper nanoparticles. (b) FTIR spectrum of the lyophilized nanoparticles and lemongrass tea (upper) and lyophilized lemongrass tea alone (lower).

absorbance is attributed to scattering due to the slight turbidity of the lemongrass tea; however, the tea itself does not generate spectral features in UV−vis. A lack of surface plasmon resonance peaks in the visible spectrum, as shown in Figure 1a, may be attributed to copper nanoparticles with diameters less than about 5 nm.[47−49] Ultrasmall nanoparticles and atomically precise clusters lose their visible extinction features as a function of size.[30−32,47−52] While larger copper nanoparticles and coupled ultrasmall copper particles display a strong plasmon peak at 560−570 nm, isolated ultrasmall copper nanoparticles do not show strong plasmon peaks. Very small peaks or shoulders have been observed; however, it is common that ultrasmall copper nanoparticles lack a clear extinction peak in the visible range. Depending on the particle size, copper can display varying absorbance intensities at various wavelengths of maximum absorbance,[47−49,51] and rapidly increasing absorbance at wavelengths below ∼350 nm, such as observed here, has been observed previously with copper nanoparticles that do not show surface plasmon resonance in the visible range.[31,32,47,48]

FTIR was used to gain understanding of the functional groups that are involved in the nanoparticle reduction and apparent oxidative stability and to compare the lemongrass tea to other plant-based nanoparticle syntheses. Representative spectra of the lyophilized lemongrass−nanoparticle mixture and lemongrass tea are shown in Figure 1b. The general features of the spectra are common to spectra of plant materials used in nanoparticle synthesis reported elsewhere.[39,53−55] Three bands appear in the both spectra between 1054 and 1616 cm^{-1}. A broad band also appears near 3400 cm^{-1}, and two less intense

and narrower bands appear between 2849 and 2939 cm^{-1}. The variety of N- and O-containing functional groups as well as the possible C−C and C−H result in several possible assignments for the bands observed. The broad bands observed near 3400 cm^{-1} are likely due to −O−H stretch from hydroxyl groups expected to be present in the plant material, such as sugars or polyphenols. The band may also be at least partly due to incorporated water. Even though the samples were lyophilized and stored in a desiccator prior to analysis, the dried solids are hygroscopic. The bands appearing between 2849 and 2939 cm^{-1} are C−H stretching modes from hydrocarbon chains. Bands due to C−O−H bending vibrations appear near 1420 cm^{-1}. The amide I band from protein carbonyl stretch appears at 1616 cm^{-1} and has been noted elsewhere in similar plant-based nanoparticle analyses.[53,54] All of the noted features could result from the polyphenols, proteins, and small molecules likely to be in the plant tea mixture. Given that similar features appear in the spectra of a variety of plant tea reducing agents, similar functional groups and structures are likely responsible for the formation and capping of nanoparticles prepared in this manner.

Analysis with (scanning) transmission electron microscopy (STEM) and HR-TEM shows finely divided and well dispersed particles with little evidence of aggregation. In the high-angle annular dark field (HAADF) image in Figure 2a, the particles appear as bright spots. The average diameter of the nanoparticles was found to be 2.90 ± 0.64 nm (averaged over three batches), and the population distribution is given in Figure 2b.

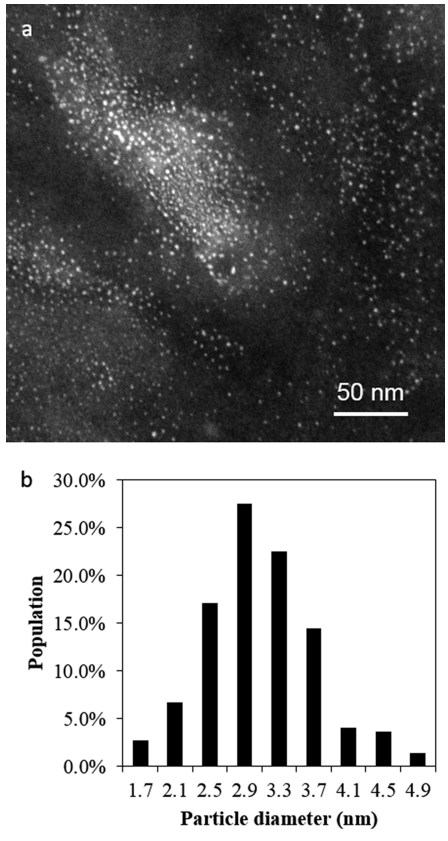

Figure 2. (a) HAADF STEM image of ultrasmall Cu nanoparticles in which the particles appear as bright spots. (b) Population distribution for three batches of the nanoparticles. Average diameter is 2.90 ± 0.64 nm.

Atomic absorbance spectroscopy (AAS) of the centrifuged and acid-digested samples resulted in an average total copper recovery of ∼99.0%. The pelleted materials contained 69.5 ± 0.9% of the total copper added as precursor, and the supernatant contained the balance with 29.5 ± 2.9% of the total copper. Nanoparticle yields are not routinely reported due to difficulties in obtaining reliable quantitative results,[56] and the results reported here may not be fully representative of an inherently complex system. Recovering nearly all of the copper added as precursor in the final sol is encouraging; however, it is more challenging to determine if the pellet is purely copper in the form of ultrasmall nanoparticles and if the supernatant only contains unreduced precursor with no particles, particularly because the nanoparticles are not plasmonic.

The nanoparticle lattice structure was imaged with HR-TEM, as shown in Figure 3a and b. The images themselves and the

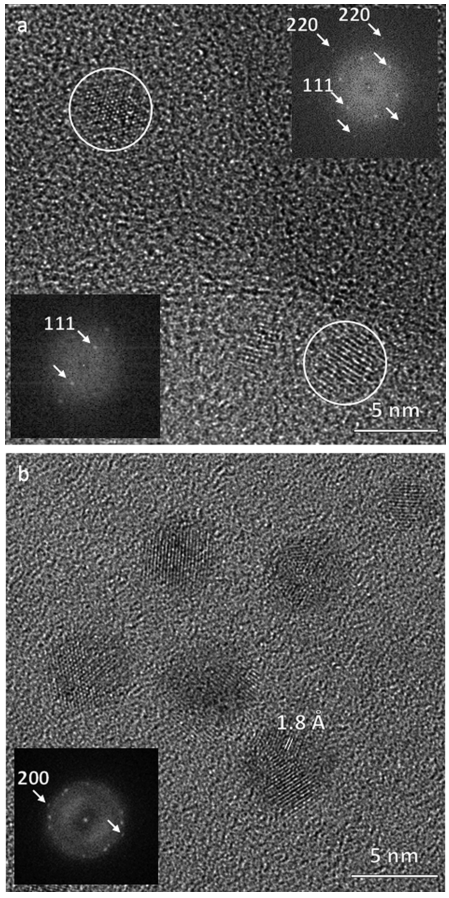

Figure 3. HR-TEM images show the lattice structure of the particles. Insets are Fourier transforms (FTs) of (a) individual circled particles beside the (FTs) and (b) the six particles in the image. In panel (a), spots in the FTs representing (220) and (111) lattice spacings are noted. In panel (b), the spots representing the (200) lattice spacing are indicated with arrows in the Fourier transform, and the associated 1.8 Å spacing on the corresponding particle is noted.

Fourier transforms of the particles (inset images) show that the individual particles are single crystalline. In the Fourier transforms, the distance of the surrounding spots from the center spot allows for the average lattice spacing to be calculated in the parent HR-TEM image. Numerous examples of copper (111) lattice spacings of 2.1 Å were found among the particles analyzed (JCPDS card 04-0836). The strong presence

of 2.1 Å lattice spacings is indicative of Cu. The Cu (220) lattice spacing of 1.3 Å and the (220) lattice spacing of 1.8 Å were also found via Fourier transform analysis of the HR-TEM images. Surprisingly, lattice spacings indicative of oxidized copper, CuO, and Cu_2O, for example, were not found. The (111) spacings of CuO and Cu_2O are 2.32 and 2.47 Å, respectively, and are sufficiently different from the lattice spacings for Cu so that oxidized copper should not be easily confused with fully reduced copper (JCPDS cards 48-157 and 05-0667, respectively).

If the ~69.5% yield, as determined by AAS, is considered with the average nanoparticle diameter of 2.90 nm, an approximate nanoparticle concentration can be calculated. Assuming a 74% packing efficiency of copper in an fcc lattice with copper atomic diameter of 2.55 Å and using the concentration of copper precursor in the reaction mixture, a final nanoparticle concentration of approximately 0.45 μM is obtained.

Components of the lemongrass tea may offer the copper nanoparticles protection against aggregation and oxidation. As noted by others, copper nanoparticles may be reduced and subsequently protected against oxidation by lactic acid[57] or ascorbic acid.[41,58,59] Each acid, when present in a copper nanoparticle sol, provides an antioxidant capacity, and the nanoparticles remain in the fully reduced state. The addition of bulky capping agents, such as polyethylene glycol (PEG)[58] or polyvinylpyrrolidone (PVP),[59,60] can prevent oxidation as well as particle aggregation. Similar to the work presented here, the ascorbic acid-PEG copper nanoparticle syntheses did not require deoxygenation of the reaction mixture to produce or retain Cu (0) nanoparticles.

In an attempt to separate the nanoparticles from the complex lemongrass tea mixture, the particles were transferred to hexane when derivatized with ODT. Due to the nonplasmonic nature of the particles, TEM was used to determine if nanoparticles were transferred to the hexane phase from the as-synthesized aqueous phase. A nickel TEM grid was dipped into the hexane layer of the two-phase system and allowed to dry. As shown in Figure 4a and b, particles were found on the grid and were confirmed to contain copper through in situ EDS. Carbon and nickel are from the grid. Sulfur is attributed to the sulfur groups on the ODT. Sulfur is not detected in EDS spectra of the as-synthesized Cu nanoparticles nor is it detected in the lemongrass tea sample that was used as a background (Figure S1, Supporting Information). Chlorine is attributed to chloride salts—particularly KCl—found in the lemongrass tea. Other elements detected in the extracted sample, such as Si and P, are also detected in the lemongrass background. The extraction with ODT reduces the relative intensities of the elements attributed to the lemongrass tea. This extraction method may allow for further concentration of the nanoparticles and will likely simplify sample preparation for further analyses and evaluation of properties.

By considering the FTIR spectra with the EDS data, nitrogen and sulfur functional groups are not indicated as being directly involved with the formation of the ultrasmall copper nanoparticles. Both FTIR and EDS (Kα emission 0.525 keV) indicate the presence of oxygen. Nitrogen is not evident in EDS (Kα emission 0.392 keV) and is notably absent between the large carbon Kα emission (0.277 keV) and the sharp oxygen Kα emission. If nitrogen is present, it is at relatively low concentration, and its signal is lost between the larger carbon and oxygen emission peaks in the EDS spectra. Sulfur (Kα emission 2.307 keV), which is not observed in the as-synthesized nanoparticle samples, is observed at relatively low levels in the lemongrass background and is relatively abundant in the ODT-derivatized sample. Further analyses will be pursued to confirm the role of oxygen-containing functional groups in the formation and protection of the copper nanoparticles; however, the related work with ascorbic acid,[41,58,59] PEG,[58] and PVP[59] supports the assertion that carboxylic acids, hydroxyls, and other oxygen-containing groups are important in this system as well and could account for the nanoparticles' observed oxidative and physical stability.

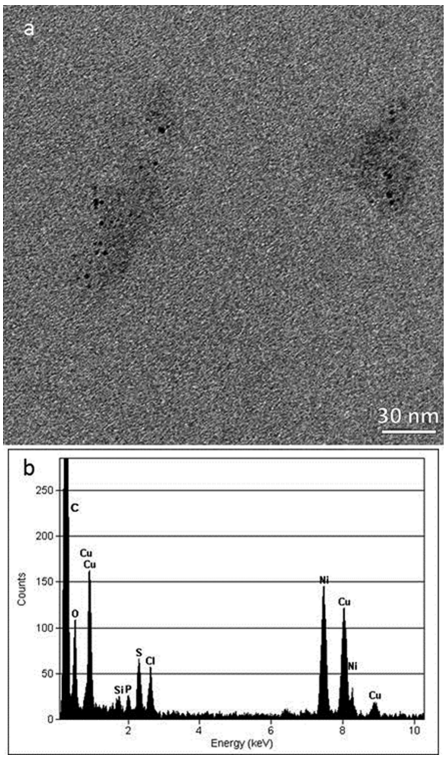

Figure 4. (a) TEM image of ultrasmall Cu nanoparticles that were transferred to hexane by first derivatizing the particles with ODT. (b) EDS of the particles shown in panel (a). Cu is the major component not attributed to the TEM grid. Sulfur is attributed to ODT and is not found in the as-synthesized sol and only in very low levels in the lemongrass background. These and other elements present in the lemongrass background are decreased by transferring the particles to hexane with ODT.

Shells of copper oxide on copper nanoparticles have been reported and, along with small particle size, contribute to diminishment of the surface plasmon in the visible range.[30,31,47,61] As discussed above, copper oxide was not found via analysis of the nanoparticle lattice, and there is no evidence in the UV−vis spectrum (Figure 1a) of copper oxide bandgap transitions in the 700−800 nm range.[31,61]

The specific origin of oxygen in the EDS spectra is indeterminate at this time, but it is clearly present at significant levels in the lemongrass-only sample (Figure S1, Supporting Information), and oxygen-containing functional groups are indicated in the FTIR spectra of both the freeze-dried lemongrass and copper nanoparticle sample (Figure 1b). Continuing work with our system aims to identify specific compounds, in which oxygen-containing functional groups seem to be indicated, that reduce the copper and protect it from oxidation.

CONCLUSIONS

Lemongrass tea has been shown to reduce copper(II) ions to form ultrasmall copper nanoparticles. The approximately spherical nanoparticles have an average diameter of 2.90 ± 0.64 nm, a size that diminishes the local surface plasmon resonance observed in larger copper nanoparticles. FTIR analysis of the freeze-dried lemongrass tea and nanoparticles shows several features common to plant-based reducing agent mixtures for the formation of nanoparticles, including the presence of oxygen-containing functional groups. Analysis of HR-TEM images and their Fourier transforms shows that the synthesized particles are largely single crystalline. The Fourier analysis also confirms that the particles are composed of copper rather than a copper oxide. Lattice spacings were determined to match the (111), (200), and (220) lattice spacing of Cu. Lattice spacings associated with copper oxides were not found. The particles are stable in aqueous solution but may be transferred to hexane with the addition of 1-octadecanethiol, as confirmed with TEM-EDS analysis. The transfer to hexane also reduced the relative amounts of elements attributed to the lemongrass, providing a less complex sample matrix. No special conditions, such as solvent deoxygenation, were maintained to form or preserve the Cu in aqueous solution. Work to identify the components of the lemongrass tea that reduce the copper nanoparticles and appear to protect them from further oxidation is ongoing.

ASSOCIATED CONTENT

Supporting Information

Figure S1: EDS spectra of an additional particle point analysis of copper nanoparticles transferred to hexane, as-synthesized aqueous copper sol, and lemongrass with no added copper precursor. This material is available free of charge via the Internet at http://pubs.acs.org.

AUTHOR INFORMATION

Corresponding Author

*E-mail: stangels@dickinson.edu. Phone: (717) 254-8957. Fax: (717) 245-1995.

Present Addresses

Aaron D. Brumbaugh: School of Medicine, New York Medical College, Valhalla, New York 10595, United States.

Katelyn A. Cohen: Jefferson Medical College, Thomas Jefferson University, Philadelphia, Pennsylvania 19107, United States.

Author Contributions

The manuscript was written through contributions of all authors. All authors have given approval to the final version of the manuscript.

Notes

The authors declare no competing financial interest.

ACKNOWLEDGMENTS

The authors acknowledge support for this work from the following: Dickinson College's R&D Student-Faculty Research (SFR) grant and sabbatical support and the Dickinson Center for Sustainability Education (CSE) SFR, American Association of University Women (AAUW) U.S. Postdoctoral Research Fellowship, and Penn State Center for Nanoscale Science through NSF-MRSEC (DMR-0820404) as part of the MRFN faculty fellow program. We also thank Ke Wang, Trevor Clark, and Jennifer Gray at Penn State Materials Characterization Laboratory for kind assistance with TEM. We are grateful to our reviewers for helpful comments.

REFERENCES

(1) Benavente, E.; Lozano, H.; Gonzalez, G. Fabrication of copper nanoparticles: Advances in synthesis, morphology control, and chemical stability. *Recent Pat. Nanotechnol.* **2013**, *7*, 108−132.

(2) Prucek, R.; Kvitek, L.; Panacek, A.; Vancurova, L.; Soukupova, J.; Jancik, D.; Zboril, R. Polyacrylate-assisted synthesis of stable copper nanoparticles and copper(I) oxide nanocubes with high catalytic efficiency. *J. Mater. Chem.* **2009**, *19*, 8463−8469.

(3) Mo, L.; Kawi, S. An in situ self-assembled core-shell precursor route to prepare ultrasmall copper nanoparticles on silica catalysts. *J. Mater. Chem. A* **2014**, *2*, 7837−7844.

(4) Nian, J.; Chen, S.; Tsai, C.; Teng, H. Structural feature and catalytic performance of Cu species distributed over TiO_2 nanotubes. *J. Phys. Chem. B* **2006**, *110*, 25817−25824.

(5) Ren, J.; Liu, S.; Li, Z.; Xie, K. Structural feature and catalytic performance of Cu-SiO_2-TiO_2 cogelled xerogel catalysts for oxidative carbonylation of methanol to dimethyl carbonate. *Catal. Commun.* **2011**, *12*, 357−361.

(6) Wang, Y.; Biradar, A. V.; Wang, G.; Sharma, K. K.; Duncan, C. T.; Rangan, S.; Asefa, T. Controlled synthesis of water-dispersible faceted crystalline copper nanoparticles and their catalytic properties. *Chem.−Eur. J.* **2010**, *16*, 10735−10743.

(7) Yin, A.; Guo, X.; Dai, W.; Fan, K. The nature of active copper species in Cu-HMS catalyst for hydrogenation of dimethyl oxalate to ethylene glycol: New insights on the synergetic effect between Cu^0 and Cu^+. *J. Phys. Chem. C* **2009**, *113*, 11003−11013.

(8) Sun, Q.; Sun, X.; Dong, H.; Zhang, Q.; Dong, L. Copper quantum dots on TiO_2: A high-performance, low-cost, and nontoxic photovoltaic material. *J. Renewable Sustainable Energy* **2013**, *5*, 021413.

(9) Leifert, A.; Pan-Bartnek, Y.; Simon, U.; Jahnen-Dechent, W. Molecularly stabilised ultrasmall gold nanoparticles: Synthesis, characterization and bioactivity. *Nanoscale* **2013**, *5*, 6224−6242.

(10) Huang, K.; Ma, H.; Liu, J.; Huo, S.; Kumar, A.; Wei, T.; Zhang, X.; Jin, S.; Gan, Y.; Wang, P. C.; He, S.; Zhang, X.; Liang, X. Size-dependent localization and penetration of ultrasmall gold nanoparticles in cancer cells, multicellular spheroids, and tumors in vivo. *ACS Nano* **2012**, *6*, 4483−4493.

(11) Kloust, H.; Poeselt, E.; Kappen, S.; Schmidtke, C.; Kornowski, A.; Pauer, W.; Moritz, H.; Weller, H. Ultrasmall biocompatible nanocomposites: A new approach using seeded emulsion polymerization for the encapsulation of nanocrystals. *Langmuir* **2012**, *28*, 7276−7281.

(12) Xu, Y.; Liu, Q.; Zhu, Y.; Liu, Y.; Langrock, A.; Zachariah, M. R.; Wang, C. Uniform nano-Sn/C composite anodes for lithium ion batteries. *Nano Lett.* **2013**, *13*, 470−474.

(13) Bazargan, S.; Heinig, N. F.; Rios, J. F.; Leung, K. T. Electronic transport in tin(IV) oxide nanocrystalline films: Two-medium transport with three-dimensional variable-range hopping mechanism for the ultrasmall nanocrystallite size regime. *J. Phys. Chem. C* **2012**, *116*, 4979−4985.

(14) Ostrowski, A. D.; Chan, E. M.; Gargas, D. J.; Katz, E. M.; Han, G.; Schuck, P. J.; Milliron, D. J.; Cohen, B. E. Controlled synthesis and single-particle imaging of bright, sub-10 nm lanthanide-doped upconverting nanocrystals. *ACS Nano* **2012**, *6*, 2686−2692.

(15) Ma, K.; Werner-Zwanziger, U.; Zwanziger, J.; Wiesner, U. Controlling growth of ultrasmall sub-10 nm fluorescent mesoporous silica nanoparticles. *Chem. Mater.* **2013**, *25*, 677−691.

(16) Kharissova, O. V.; Kharisov, B. I.; Manuel Jimenez-Perez, V.; Munoz Flores, B.; Ortiz Mendez, U. Ultrasmall particles and nanocomposites: State of the art. *RSC Adv.* **2013**, *3*, 22648−22682.

(17) Chen, G.; Qiu, H.; Fan, R.; Hao, S.; Tan, S.; Yang, C.; Han, G. Lanthanide-doped ultrasmall yttrium fluoride nanoparticles with enhanced multicolor upconversion photoluminescence. *J. Mater. Chem.* **2012**, *22*, 20190−20196.

(18) Costo, R.; Bello, V.; Robic, C.; Port, M.; Marco, J. F.; Puerto Morales, M.; Veintemillas-Verdaguer, S. Ultrasmall iron oxide

nanoparticles for biomedical applications: Improving the colloidal and magnetic properties. *Langmuir* **2012**, *28*, 178−185.
(19) Gao, G.; Wu, H.; Zhang, Y.; Luo, T.; Feng, L.; Huang, P.; He, M.; Cui, D. Synthesis of ultrasmall nucleotide-functionalized superparamagnetic gamma-Fe_2O_3 nanoparticles. *CrystEngComm* **2011**, *13*, 4810−4813.
(20) Zhu, Z.; Wang, S.; Du, J.; Jin, Q.; Zhang, T.; Cheng, F.; Chen, J. Ultrasmall Sn nanoparticles embedded in nitrogen-doped porous carbon as high-performance anode for lithium-ion batteries. *Nano Lett.* **2014**, *14*, 153−157.
(21) Zedan, A. F.; Moussa, S.; Terner, J.; Atkinson, G.; El-Shall, M. S. Ultrasmall gold nanoparticles anchored to graphene and enhanced photothermal effects by laser irradiation of gold nanostructures in graphene oxide solutions. *ACS Nano* **2013**, *7*, 627−636.
(22) Walsh, M. J.; Yoshida, K.; Kuwabara, A.; Pay, M. L.; Gai, P. L.; Boyes, E. D. On the structural origin of the catalytic properties of inherently strained ultrasmall decahedral gold nanoparticles. *Nano Lett.* **2012**, *12*, 2027−2031.
(23) Liu, X.; Cao, Y.; Peng, H.; Qian, H.; Yang, X.; Zhang, H. Silica/ultrasmall Ag composite microspheres: Facile synthesis, characterization and antibacterial and catalytic performance. *CrystEngComm* **2014**, *16*, 2365−2370.
(24) Cheng, Z.; Zhong, H.; Xu, J.; Chu, X.; Song, Y.; Xu, M.; Huang, H. Facile fabrication of ultrasmall and uniform copper nanoparticles. *Mater. Lett.* **2011**, *65*, 3005−3008.
(25) Delalande, M.; Guinel, M. J.; Allard, L. F.; Delattre, A.; Le Bris, R.; Samson, Y.; Bayle-Guillemaud, P.; Reiss, P. L1(0) ordering of ultrasmall FePt nanoparticles revealed by TEM in situ annealing. *J. Phys. Chem. C* **2012**, *116*, 6866−6872.
(26) Kim, B. H.; Hackett, M. J.; Park, J.; Hyeon, T. Synthesis, characterization, and application of ultrasmall nanoparticles. *Chem. Mater.* **2014**, *26*, 59−71.
(27) Pennycook, T. J.; McBride, J. R.; Rosenthal, S. J.; Pennycook, S. J.; Pantelides, S. T. Dynamic fluctuations in ultrasmall nanocrystals induce white light emission. *Nano Lett.* **2012**, *12*, 3038−3042.
(28) Li, G.; Jin, R. Atomically precise gold nanoclusters as new model catalysts. *Acc. Chem. Res.* **2013**, *46*, 1749−1758.
(29) Shang, L.; Brandholt, S.; Stockmar, F.; Trouillet, V.; Bruns, M.; Nienhaus, G. U. Effect of protein adsorption on the fluorescence of ultrasmall gold nanoclusters. *Small* **2012**, *8*, 661−665.
(30) Brege, J. J.; Hamilton, C. E.; Crouse, C. A.; Barron, A. R. Ultrasmall copper nanoparticles from a hydrophobically immobilized surfactant template. *Nano Lett.* **2009**, *9*, 2239−2242.
(31) Ghosh, S. K.; Rahman, D. S.; Ali, A. L.; Kalita, A. Surface plasmon tunability and emission sensitivity of ultrasmall fluorescent copper nanoclusters. *Plasmonics* **2013**, *8*, 1457−1468.
(32) Biswas, S.; Miller, J. T.; Li, Y.; Nandakumar, K.; Kumar, C. S. S. R. Developing a millifluidic platform for the synthesis of ultrasmall nanoclusters: Ultrasmall copper nanoclusters as a case study. *Small* **2012**, *8*, 688−698.
(33) Kharissova, O. V.; Dias, H. V. R.; Kharisov, B. I.; Pérez, B. O.; Pérez, V. M. J. The greener synthesis of nanoparticles. *Trends Biotechnol.* **2013**, *31*, 240−248.
(34) Akhtar, M. S.; Panwar, J.; Yun, Y. Biogenic synthesis of metallic nanoparticles by plant extracts. *ACS Sustainable Chem. Eng.* **2013**, *1*, 591−602.
(35) AbdelHamid, A. A.; Al-Ghobashy, M.; Fawzy, M.; Mohamed, M. B.; Abdel-Mottaleb, M. Phytosynthesis of Au, Ag, and Au-Ag bimetallic nanoparticles using aqueous extract of sago pondweed (*Potamogeton pectinatus* L.). *ACS Sustainable Chem. Eng.* **2013**, *1*, 1520−1529.
(36) Kahrilas, G. A.; Wally, L. M.; Fredrick, S. J.; Hiskey, M.; Prieto, A. L.; Owens, J. E. Microwave-assisted green synthesis of silver nanoparticles using orange peel extract. *ACS Sustainable Chem. Eng.* **2013**, *2*, 367−376.
(37) St. Angelo, S. K.; Hartz, E. L. Ginkgo as a green reducing agent for gold nanoparticles and nanoplatelets. *Int. J. Green Nanotechnol.* **2012**, *4*, 111−116.
(38) Tokarek, K.; Hueso, J. L.; Kustrowski, P.; Stochel, G.; Kyziol, A. Green synthesis of chitosan-stabilized copper nanoparticles. *Eur. J. Inorg. Chem.* **2013**, *2013*, 4940−4947.
(39) Sastry, A. B. S.; Aamanchi, R. B. K.; Prasad, C. S. R. L.; Murty, B. S. Large-scale green synthesis of Cu nanoparticles. *Environ. Chem. Lett.* **2013**, *11*, 183−187.
(40) Bendi, R.; Imae, T. Renewable catalyst with Cu nanoparticles embedded into cellulose nano-fiber film. *RSC Adv.* **2013**, *3*, 16279−16282.
(41) Xiong, J.; Wang, Y.; Xue, Q.; Wu, X. Synthesis of highly stable dispersions of nanosized copper particles using L-ascorbic acid. *Green Chem.* **2011**, *13*, 900−904.
(42) Santos, E. d. B.; Sigoli, F. A.; Mazali, I. O. Metallic Cu nanoparticles dispersed into porous glass: A simple green chemistry approach to prepare SERS substrates. *Mater. Lett.* **2013**, *108*, 172−175.
(43) Shankar, S. S.; Rai, A.; Ankamwar, B.; Singh, A.; Ahmad, A.; Sastry, M. Biological synthesis of triangular gold nanoprisms. *Nat. Mater.* **2004**, *3*, 482−488.
(44) Rai, A.; Singh, A.; Ahmad, A.; Sastry, M. Role of halide ions and temperature on the morphology of biologically synthesized gold nanotriangles. *Langmuir* **2006**, *22*, 736−741.
(45) Rai, A.; Chaudhary, M.; Ahmad, A.; Bhargava, U.; Sastry, M. Synthesis of triangular Au core-Ag shell nanoparticles. *Mater. Res. Bull.* **2007**, *42*, 1212−1220.
(46) Masurkar, S. A.; Chaudhari, P. R.; Shidore, V. B.; Kamble, S. P. Rapid biosynthesis of silver nanoparticles using *Cymbopogan citratus* (lemongrass) and its antimicrobial activity. *Nano-Micro Letters* **2011**, *3*, 189−194.
(47) Singh, M.; Sinha, I.; Premkumar, M.; Singh, A. K.; Mandal, R. K. Structural and surface plasmon behavior of Cu nanoparticles using different stabilizers. *Colloid Surf., A* **2010**, *359*, 88−94.
(48) Siwach, O. P.; Sen, P. Synthesis and study of fluorescence properties of Cu nanoparticles. *J. Nanopart. Res.* **2008**, *10*, 107−114.
(49) Pileni, M. P.; Lisiecki, I. Nanometer metallic copper particle synthesis in reverse micelles. *Colloids Surf., A* **1993**, *80*, 63−68.
(50) Wei, W.; Lu, Y.; Chen, W.; Chen, S. One-pot synthesis, photoluminescence, and electrocatalytic properties of subnanometer-sized copper clusters. *J. Am. Chem. Soc.* **2011**, *133*, 2060−2063.
(51) Vazquez-Vazquez, C.; Banobre-Lopez, M.; Mitra, A.; Arturo Lopez-Quintela, M.; Rivas, J. Synthesis of small atomic copper clusters in microemulsions. *Langmuir* **2009**, *25*, 8208−8216.
(52) Niranjan, M. K.; Chakraborty, J. Synthesis of oxidation resistant copper nanoparticles in aqueous phase and efficient phase transfer of particles using alkanethiol. *Colloids Surf., A* **2012**, *407*, 58−63.
(53) Narayanan, K. B.; Sakthivel, N. Coriander leaf mediated biosynthesis of gold nanoparticles. *Mater. Lett.* **2008**, *62*, 4588−4590.
(54) Sheny, D. S.; Mathew, J.; Philip, D. Phytosynthesis of Au, Ag and Au−Ag bimetallic nanoparticles using aqueous extract and dried leaf of *Anacardium occidentale*. *Spectrochim. Acta, Part A* **2011**, *79*, 254−262.
(55) Dubey, S. P.; Lahtinen, M.; Sillanpaa, M. Green synthesis and characterizations of silver and gold nanoparticles using leaf extract of *Rosa rugosa*. *Colloids Surf., A* **2010**, *364*, 34−41.
(56) Jia, H.; Gao, X.; Chen, Z.; Liu, G.; Zhang, X.; Yan, H.; Zhou, H.; Zheng, L. The high yield synthesis and characterization of gold nanoparticles with superior stability and their catalytic activity. *CrystEngComm* **2012**, *14*, 7600−7606.
(57) Deng, D.; Cheng, Y.; Jin, Y.; Qi, T.; Xiao, F. Antioxidative effect of lactic acid-stabilized copper nanoparticles prepared in aqueous solution. *J. Mater. Chem.* **2012**, *22*, 23989−23995.
(58) Zhang, Y.; Zhu, P.; Li, G.; Zhao, T.; Fu, X.; Sun, R.; Zhou, F.; Wong, C. Facile preparation of monodisperse, impurity-free, and antioxidation copper nanoparticles on a large scale for application in conductive ink. *ACS Appl. Mater. Interfaces* **2014**, *6*, 560−567.
(59) Yu, W.; Xie, H.; Chen, L.; Li, Y.; Zhang, C. Synthesis and characterization of monodispersed copper colloids in polar solvents. *Nanoscale Res. Lett.* **2009**, *4*, 465−470.

(60) Engels, V.; Benaskar, F.; Jefferson, D. A.; Johnson, B. F. G.; Wheatley, A. E. H. Nanoparticulate copper - routes towards oxidative stability. *Dalton Trans.* **2010**, *39*, 6496−6502.
(61) Rice, K. P.; Walker, E. J., Jr.; Stoykovich, M. P.; Saunders, A. E. Solvent-dependent surface plasmon response and oxidation of copper nanocrystals. *J. Phys. Chem. C* **2011**, *115*, 1793−1799.